Extensible-Link Kinematic Model for Characterizing and Optimizing Compliant Mechanism Motion

Justin Beroz[1]
Mechanosynthesis Group
Department of Mechanical Engineering,
Massachusetts Institute of Technology,
Cambridge, MA 02139
e-mail: jberoz@mit.edu

Shorya Awtar
Precision Systems Design Laboratory,
Department of Mechanical Engineering,
University of Michigan,
Ann Arbor, MI 48109
e-mail: awtar@umich.edu

A. John Hart
Mechanosynthesis Group
Department of Mechanical Engineering,
Massachusetts Institute of Technology,
Cambridge, MA 02139
e-mail: ajhart@mit.edu

We present an analytical model for characterizing the motion trajectory of an arbitrary planar compliant mechanism. Model development consists of identifying particular material points and their connecting vectorial lengths in a manner that represents the mechanism topology; whereby these lengths may extend over the course of actuation to account for the elastic deformation of the compliant mechanism. The motion trajectory is represented within the model as an analytical function in terms of these vectorial lengths, whereby its Taylor series expansion constitutes a parametric formulation composed of load-independent and load-dependent terms. This adds insight to the process for designing compliant mechanisms for high-accuracy motion applications because: (1) inspection of the load-independent terms enables determination of specific topology modifications that reduce or eliminate certain error components of the motion trajectory; and (2) the load-dependent terms reveal the polynomial orders of principally uncorrectable error components in the trajectory. The error components in the trajectory simply represent the deviation of the actual motion trajectory provided by the compliant mechanism compared to the ideally desired one. A generalized model framework is developed, and its utility demonstrated via the design of a compliant microgripper with straight-line parallel jaw motion. The model enables analytical determination of all geometric modifications for minimizing the error trajectory of the jaw, and prediction of the polynomial order of the uncorrectable trajectory components. The jaw trajectory is then optimized using iterative finite elements simulations until the polynomial order of the uncorrectable trajectory component becomes apparent; this reduces the error in the jaw trajectory by 2 orders of magnitude over the prescribed jaw stroke. This model serves to streamline the design process by identifying the load-dependent sources of trajectory error in a compliant mechanism, and thereby the limits with which this error may be redressed by topology modification. [DOI: 10.1115/1.4026269]

Keywords: compliant mechanism, accuracy, path generation, flexure, microgripper, topology optimization, extensible-link, kinematic model, load dependency

1 Introduction

By virtue of having zero backlash and no Coulomb friction, compliant mechanisms are particularly suited for executing precision tasks requiring high-accuracy motion, including micro- and nano-manipulation [1–4], mechanical transduction [5,6], component alignment [7–9], and metrology [10,11]. Moreover, compliant mechanisms are ubiquitous in microfabricated devices and systems because monolithic construction is easily achieved by lithography and etching of silicon wafers [12].

A compliant mechanism is typically designed to provide a desired motion trajectory within a set of constraints, which may include the available mechanism area (i.e., the "footprint"), the means of actuation, the material properties, and the capabilities of the fabrication process. As shown schematically in Fig. 1, a compliant mechanism must be designed to fit within the mechanism area, be anchored at the available ground location(s), and comprise the "trajectory body," with respect to which the desired motion trajectory, $\Omega_d(\xi)$, is defined. This trajectory, $\Omega_d(\xi)$, is the translation of a particular material point on, or the translation/rotation of, the trajectory body; and is traced out by actuation of the compliant mechanism via an applied load. This load may be applied by various means, including: displacement of a linear/rotary actuator; induced strain of a portion of the compliant mechanism (thermal, piezoelectric, etc.); or by an applied electrostatic and/or electro-magnetic body force (comb-drive actuator, voice-coil actuator, etc.). The desired trajectory can be expressed as a function of a stroke parameter, ξ, which may represent either the applied load or the motion component of a body in the compliant mechanism that is critical to defining the desired trajectory. Here, ξ_0 corresponds to the undeformed state of the compliant mechanism. The design task for high-accuracy motion applications represented by Fig. 1 is therefore to design a compliant mechanism that achieves the desired trajectory, $\Omega_d(\xi)$, given a prescribed mechanism area (dashed rectangle), ground location, and load application.

An important part of this design process is to evaluate a candidate compliant mechanism by determining the accuracy with which it can trace the desired trajectory. This evaluation is important because the extent to which the desired motion trajectory can be realized via the compliant mechanism determines its efficacy for the motion application. Generally speaking, this motion trajectory is dependent on the load application, as well as the

[1]Corresponding author.

Contributed by the Mechanisms and Robotics Committee of ASME for publication in the Journal of Mechanical Design. Manuscript received March 9, 2013; final manuscript received December 12, 2013; published online January 10, 2014. Assoc. Editor: Oscar Altuzarra.

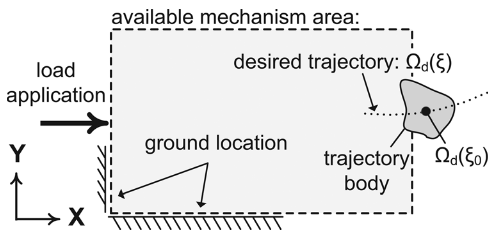

Fig. 1 Representative compliant mechanism design scenario for high-accuracy motion applications

mechanism topology and shape. These dependencies are coupled, which adds difficulty to understanding and predicting the exact motion characteristics of the mechanism.

Topology symmetry is often utilized to avoid this complication, yet this is only feasible where there is adequate available mechanism area, and only for certain desired trajectories (i.e., straight lines). Application-specific requirements often place strict limitations on some aspects of the design domain, such as: mechanism size; location and orientation of the applied load; type of actuator for applying the load; available ground locations; location of, and attachment points to, the trajectory body; and material selection. If topology symmetry is not feasible given the shape of the desired trajectory and/or design domain limitations, the task of evaluating the trajectory accuracy of a candidate compliant mechanism is nontrivial.

Several analytical methods have been developed that address this evaluation task. For instance, the Pseudo-Rigid-Body Model (PRBM) [13,14] expedites the synthesis and design iteration of a candidate compliant mechanism topology by means of an analogous rigid-body kinematic linkage. While there are specific combinations of mechanism topologies and loading conditions for which PRBM provides an accurate trajectory approximation, the exact trajectory of a compliant mechanism need not be entirely representable by the motion of a rigid-body kinematic linkage. This is because a fixed topology rigid-body kinematic model does not adequately capture all the elastic deformations that arise over the desired range of motion of the mechanism. As an alternative to PRBM, closed-form analytical solutions have been developed for compliant mechanisms built from beam flexures to capture kinematic, elastic, and elastokinematic effects [15,16]. But this modeling effort addresses a limited range of beam shapes, and extending it to any general mechanism topology and beam shapes remains a challenge [17].

While these two analytical methods are certainly useful, the nature of the applied load, and/or the intricacy of mechanism topology/shape may not allow these methods to accurately evaluate trajectory accuracy. For such cases, finite elements (FE) modeling is the only well-established tool for quantitative evaluation of the exact trajectory accuracy of a candidate compliant mechanism. FE modeling is therefore often utilized in conjunction with the aforementioned analytical models, as well as with recursive numerical procedures that integrate one or more the following design steps: (1) synthesis of a candidate compliant mechanism topology; (2) evaluation of the mechanism's trajectory accuracy; and (3) optimization by means of modifying the mechanism topology and shape so as to minimize trajectory inaccuracy. Approaches include multi-criteria [18,19], continuous material distribution [20,21], and genetic [22,23] numerical optimization algorithms. With sufficient FE simulation iterations, it is possible, in many cases, to modify a candidate compliant mechanism's topology and shape so that it exhibits sufficient trajectory accuracy. However, a *residual* error trajectory often exists *after* optimization, in terms of the mechanism's ability to trace the desired motion trajectory.

Importantly, neither FE modeling nor the recursive optimization methods elicit an intuitive understanding regarding the existence, magnitude, or characteristic form of this residual error trajectory. The designer is therefore left without a clear understanding regarding *why* this residual error exists, or to what extent it may, in principle, be redressed. It is possible for considerable time to be spent modifying the mechanism's topology and shape in an attempt to redress this residual error trajectory, which may in fact be fundamentally uncorrectable due to some aspect of the mechanism topology. If unsuccessful in sufficiently reducing the error trajectory, and being no more informed as to its source within the compliant mechanism, the designer is left to simply "guess" either: (1) a new model if synthesizing by PRBM, or (2) new/additional initial conditions if synthesizing by a recursive numerical method.

To address this difficulty, we have developed an analytical approach that aids in understanding and evaluating the motion trajectory characteristics of an arbitrary planar compliant mechanism designed to accomplish a high-accuracy motion task (Fig. 1). Here, a model is created that consists of vectorial lengths spanning between selected material points which represent locations of connection between segments comprising the compliant mechanism. This may be intuitively visualized as a kinematic linkage, wherein the link lengths extend over the course of mechanism actuation to account for the elastic deformation of the compliant mechanism under the actuation loading. Within this model framework, the trajectory of the compliant mechanism, as well as extensions of the link lengths, are expressed as analytical functions with respect to a stroke parameter, ξ. A Taylor series expansion of the mechanism's trajectory is then performed with respect to ξ. This enables the trajectory to be represented by two parametrically separated motion components: *rigid-body* terms that contain only link lengths and orientations related to the undeformed state of the compliant mechanism; and *deformation* terms that, in addition, contain link extension components.

The significance of this parametric representation is that the rigid-body terms and the deformation terms comprise load-independent and load-dependent components of the compliant mechanism's motion trajectory, respectively. Because the rigid-body terms are both load-independent and solely described by the undeformed state of the compliant mechanism topology, they constitute a well-defined motion trajectory component that is entirely specifiable by design. Conversely, the deformation terms capture all load-geometry interdependencies, which necessarily arise over the course of mechanism actuation. Therefore, their magnitudes are also dependent on the mechanism's shape. Within this framework, trajectory optimization may be regarded as a procedure in which the summation of the motion contributions from the rigid-body terms and deformation terms is designed to produce the desired trajectory.

This approach can streamline the compliant mechanism design process because: (1) inspection of the rigid-body terms enables specific topology modifications to be determined for minimizing the error trajectory; and (2) the polynomial orders of principally uncorrectable trajectory components are captured by the deformation terms. While quantitative optimization of the compliant mechanism trajectory must still be performed by iterative FE simulation, all geometric correction parameters for the mechanism topology, as well as the characteristic form of the residual error trajectory, are known beforehand. As a result, some ineffective mechanism designs and topology modifications may be disregarded without FE simulation, and time is not spent attempting to redress trajectory errors that are principally uncorrectable via topology modification. This serves to reduce the amount of time and number of numerical iterations necessary to arrive at a compliant mechanism that meets or exceeds the requirements for motion accuracy.

This paper presents the analytical framework for an extensible-link kinematic model (ELKM) and details how it may be utilized, in conjunction with FE modeling, as a design and trajectory optimization method (Sec. 2). Its utility is then demonstrated in a case study (Sec. 3), where a compliant gripping mechanism with a

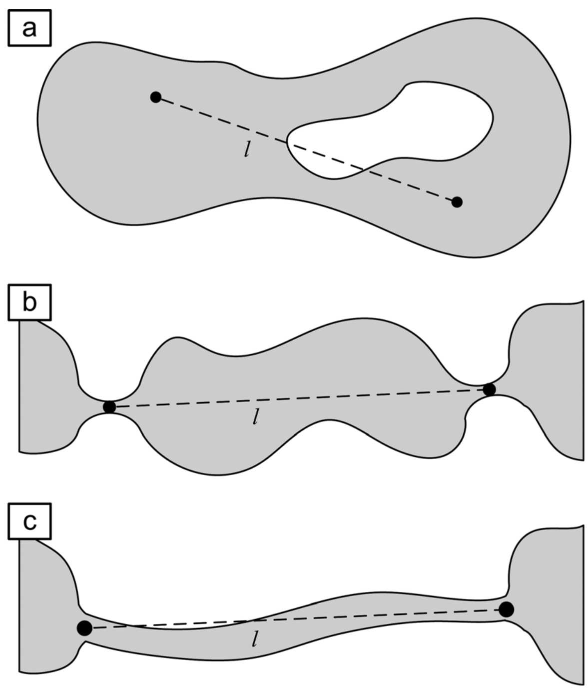

Fig. 2 (*a*) The distance, *l*, between any two material points on a continuum body admits the decomposition of Eq. (1) upon deformation due to loading. Design insights are gained by considering the distances between (*b*) compliant hinges in lumped-compliance shapes, and (*c*) end-points of compliant beams. Given a compliant mechanism, these distances, *l*, therefore represent the comprising compliant segments.

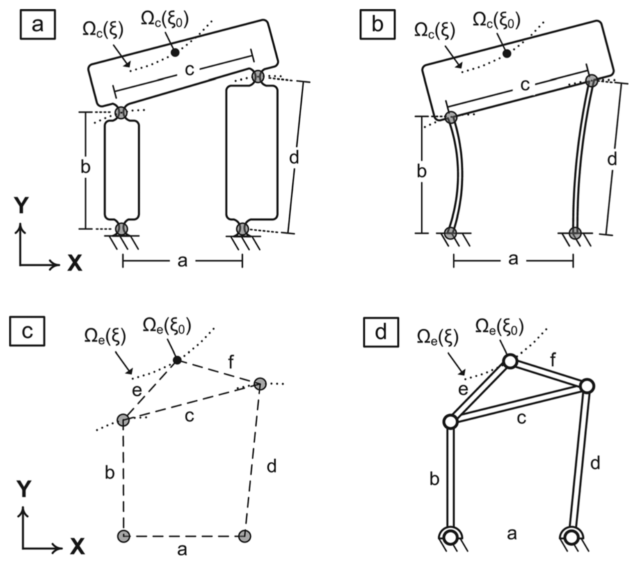

Fig. 3 Example (*a*) lumped compliance and (*b*) distributed compliance mechanisms sharing the same (*c*) topology, or equivalently, (*d*) analogous kinematic model at undeformed state, ξ_0.

straight-line parallel jaw trajectory is designed. The model is used to determine the polynomial order of the jaw's residual error trajectory, and to guide the process of optimizing the jaw motion by iterative FE simulation. The model is then summarized and discussed in context of the case study results (Sec. 4).

2 Generalized Model

2.1 Definitions and Concepts for Model Development. The desired motion trajectory, $\Omega_d(\xi)$ (denoted in a global coordinate frame), of a candidate compliant mechanism, is considered a function of stroke parameter, ξ (Fig. 1). The actual motion trajectory of this corresponding material point/body on the compliant mechanism is defined by $\Omega_c(\xi)$, which is a function of the same stroke parameter, ξ. Ideally, the compliant mechanism trajectory, $\Omega_c(\xi)$, and the desired trajectory, $\Omega_d(\xi)$, are equivalent. Therefore, the error trajectory, $\delta(\xi)$, is the difference $\Omega_c(\xi)-\Omega_d(\xi)$. Here, ξ_0 corresponds to the undeformed state of the compliant mechanism; and the deformed states within the range of actuation are defined by $\xi-\xi_0$. Because this actuation range is limited by finite material strain, it is likely that $\Omega_d(\xi)$ and $\Omega_c(\xi)$ may each be entirely represented by a single smooth continuous function. However, in general, $\Omega_d(\xi)$ and $\Omega_c(\xi)$ may each comprise a set of piece-wise smooth continuous functions defined with respect to global coordinates, whereby the following analysis would be performed for each function in the set.

Generally speaking, the distance, l, between any two material points in a deformable continuum body (Fig. 2(*a*)) may admit decomposition into (Eq. 1(*a*)): an initial length, l_0, corresponding to the undeformed state, ξ_0; and an extensible component, $f(\xi)$, expressed as a function of ξ. The extensible component simply describes the change in distance between the two material points over the course of deformation. This imparts a requirement that $f(\xi)$ be a continuous function that is equal to zero at the undeformed state, ξ_0 (Eq. 1(*b*)). Regarding the actuation of a compliant mechanism, $f(\xi)$ is attributable to the load-dependent elastic and geometric deformation that arises during loading.

$$l = l_0 + f(\xi) \tag{1a}$$

$$f(\xi_0) = 0 \tag{1b}$$

Significance, from a design perspective, is gained by selecting particular material points that represent locations of connection between segments comprising a compliant mechanism topology—namely: (1) the centers of thin compliant hinges between significantly wider sections (i.e., lumped-compliance shapes) (Fig. 2(*b*)); and (2) the end-points of compliant beams (i.e., distributed-compliance shapes) (Fig. 2(*c*)). Notice that no restriction has been placed on the deformation or shape complexity of these segments (Figs. 2(*b*) and 2(*c*)) for the decomposition of Eq. (1) to be applicable. It is in this context an "arbitrary" compliant mechanism is defined as a composition of such lumped- and distributed-compliance segments (Figs. 2(*b*) and 2(*c*)), whose configuration (i.e., location and orientation of l_0 lengths) represents the mechanism topology. The particular shape of the compliant segments affects only the extensible components, $f(\xi)$.

The complete set of selected material points for the model therefore consists of: (1) the locations of connection between compliant segments (Figs. 2(*b*) and 2(*c*)); and (2) the point defining the motion trajectory, $\Omega_c(\xi)$ (Fig. 1). The model simply comprises the connected vectorial lengths, l, which represent the material spanning between the selected material points. This is illustrated in Fig. 3 for the lumped-compliance (Fig. 3(*a*)) and distributed-compliance (Fig. 3(*b*)) shapes of an example compliant mechanism topology (Fig. 3(*c*)). Notice that the material of the trajectory body spans distances e and f as well. Because both shapes (Figs. 3(*a*) and 3(*b*)) have identical coordinate locations where the segments comprising each compliant mechanism are connected (i.e., identical topologies), both share identical model arrangements at the undeformed state, ξ_0 (i.e., the same l_0 lengths in Fig. 3(*c*)). The extensible components, $f(\xi)$, of the distances, l, comprising the models for each respective shape, however, may change differently across the range actuation, $\xi-\xi_0$.

The motions of the vectorial lengths, l, may be equivalently envisioned as an analogous kinematic mechanism (Fig. 3(*d*)), wherein extensible links are connected by pin joints residing at the selected material points (i.e., an extensible-link kinematic model). While Figs. 3(*c*) and 3(*d*) are mathematically equivalent, the latter is henceforth adopted because it provides an intuitive context—especially for visualizing the load-independent motion component in the following derivation. It also reinforces the applicability of classical kinematic analysis in performing the vector algebra to construct the model trajectory, $\Omega_e(\xi)$, in terms of the lengths and orientations of the extensible links, and as a function of the same stroke parameter, ξ (Fig. 3(*d*)). The trajectories $\Omega_e(\xi)$ and $\Omega_c(\xi)$ are therefore equivalent so long as the links in the model extend in the proper manner over the range of actuation, $\xi - \xi_0$.

While determining explicit formulas for the extensible components is generally nontrivial, the initial link lengths (i.e., l_0) are identified simply from the undeformed state of the compliant mechanism, ξ_0, according to this straightforward procedure. It will be shown that explicit formulation of the extensible components is inconsequential for distinguishing the load-independent and load-dependent motion contributions to the compliant mechanism trajectory. It is for this reason that the following derivation considers extensible length components, $\boldsymbol{f(\xi)}$, simply as smooth continuous functions, thereby granting admission to treat $\Omega_e(\xi)$ as equal to $\Omega_c(\xi)$. The design goal, again, is to have these equivalent trajectories, $\Omega_c(\xi)$ and $\Omega_e(\xi)$, match the desired trajectory, $\Omega_d(\xi)$.

2.2 Analytical Formulation. Without admitting any link length decomposition, and without loss of generality, $\Omega_e(\xi)$ may be expressed by its Taylor series expansion (Eq. (2)) with respect to ξ, about the undeformed state of the mechanism ($\xi = \xi_0$). All coefficients in the expansion, k_n, are functions of the extensible link lengths and orientations. Because the range of actuation, $\xi - \xi_0$, is finite, it can be expected that the expansion may be truncated as an ith-order polynomial, where higher-order terms are negligible.

$$\Omega_e(\xi) = \sum_{n=0}^{\infty} \frac{\Omega^{(n)}(\xi_0)}{n!}(\xi - \xi_0)^n \cong \sum_{n=0}^{i} k_n(\xi - \xi_0)^n \tag{2}$$

By now admitting the decomposition of Eq. (1), the k_n coefficients in Eq. (2) become functions of the initial lengths, l_0, as well as ξ due to the extensible components (Eq. (3)). Each k_n coefficient may therefore be represented by its respective Taylor series expansion, with respect to ξ, about the undeformed state, ξ_0. Based on the magnitude of the extensible components, $\boldsymbol{f(\xi)}$, over the stroke, the Taylor series expansion for each k_n coefficient may be truncated at some jth order, with respect to $(\xi - \xi_0)$, such that the higher-order terms, $k_{n,m>j}$, are negligible.

$$\begin{aligned}
\Omega_e(\xi) &\cong \sum_{n=0}^{i}[k_n(\xi)](\xi - \xi_0)^n = \sum_{n=0}^{i}\left[\sum_{m=0}^{\infty} k_{n,m}(\xi - \xi_0)^m\right](\xi - \xi_0)^n \\
&\cong \sum_{n=0}^{i}\sum_{m=0}^{j-n} k_{n,m}(\xi - \xi_0)^{n+m} = \Omega_{e,RB}(\xi) + \Omega_{e,D}(\xi) \\
\Omega_{e,RB}(\xi) &\triangleq \sum_{n=0}^{i} k_{n,0}(\xi - \xi_0)^n \\
\Omega_{e,D}(\xi) &\triangleq \sum_{n=0}^{i}\sum_{m=1}^{j-n} k_{n,m}(\xi - \xi_0)^{n+m}
\end{aligned} \tag{3}$$

As a result of Eq. 1(*b*), the first term in each k_n Taylor series, $k_{n,0}$, contains only l_0 lengths; these are referred to as *rigid-body* terms. Their constitution is unaffected by the extensible components, $\boldsymbol{f(\xi)}$, and therefore they collectively represent a motion trajectory component that is independent of the deformation of the compliant segments (i.e., depends only on their configuration). Furthermore, these $k_{n,0}$ terms exactly constitute the rigid-body motion trajectory, in series-representation, of the kinematic mechanism comprising only l_0 link lengths (i.e., as if all $\boldsymbol{f(\xi)}\equiv 0$); and this is denoted by $\Omega_{e,RB}(\xi)$ in Eq. (3). The order of truncation, i, is therefore determined by the number of significant terms in $\Omega_{e,RB}(\xi)$ for the range of actuation, $\xi - \xi_0$. Thus, $\Omega_{e,RB}(\xi)$ represents a component of the compliant mechanism trajectory, $\Omega_c(\xi)$, that is independent of the applied load, segment shapes, and material properties; and it may be derived simply from the compliant mechanism's undeformed state, ξ_0, using rigid-body kinematics.

All remaining terms in each k_n Taylor series, $\boldsymbol{k_{n,m>0}}$ (Eq. (3)), contain initial link lengths, l_0, as well as derivatives of the extensible components up to the mth-order, evaluated at ξ_0 (i.e., $\boldsymbol{f(\xi_0)^{(m)}}$). These are referred to as *deformation* terms. Their constitution is of a form such that they require the existence of extensible components, $\boldsymbol{f(\xi)}$, to be nonzero valued; and their magnitudes correspond to the magnitudes of the extensible component derivatives (i.e., $\boldsymbol{f(\xi_0)^{(m)}}$). This is shown explicitly in the case study (Eq. (12), Sec. 3). The motion trajectory of a compliant mechanism, $\Omega_c(\xi)$, therefore contains a load-dependent component that is represented within the model by the collective contribution of the deformation terms, $\Omega_{e,D}(\xi)$ (Eq. (3)). Hence, the values of the deformation terms: (1) capture the load-geometry interdependencies arising over the course of mechanism actuation; and (2) reflect the shape of the compliant mechanism.

The entire series expansion is now written explicitly, grouping like-ordered $k_{n,m}$ terms (Eq. (4)). For clarity, these terms are expressed as functions of $\Delta\xi$, which represents the displacement from the mechanism's undeformed state. The rigid-body, $k_{n,0}$, and deformation, $\boldsymbol{k_{n,m>0}}$ (notated in bold), terms are now represented in a parametric form showing that there is one rigid-body term per polynomial order, terminating at the ith order with respect to $\Delta\xi$. Deformation terms may range from 1st order to jth order, for some $j > i$.

$$\begin{aligned}
\Omega_e(\Delta\xi) \cong{}& [k_{0,0}] + [k_{1,0} + \boldsymbol{k_{0,1}}]\Delta\xi + [k_{2,0} + \boldsymbol{k_{1,1}} + \boldsymbol{k_{0,2}}]\Delta\xi^2 \\
&+ \ldots + \left[k_{i,0} + \sum_{n=0}^{i-1}\boldsymbol{k_{n,i-n}}\right]\Delta\xi^i + \left[\sum_{n=0}^{i}\boldsymbol{k_{n,i-n+1}}\right]\Delta\xi^{i+1} \\
&+ \ldots + \left[\sum_{n=0}^{i}\boldsymbol{k_{n,j-n}}\right]\Delta\xi^j \quad \xi \triangleq \xi_0 + \Delta\xi
\end{aligned} \tag{4}$$

Similarly, the desired motion trajectory, $\Omega_d(\xi)$, may be represented by its Taylor series expansion, with respect to ξ, about the undeformed state of the mechanism, ξ_0 (Eq. (5)).

$$\Omega_d(\Delta\xi) = \sum_{n=0}^{\infty} d_n(\Delta\xi)^n = d_0 + d_1\Delta\xi + d_2\Delta\xi^2 + \ldots \tag{5}$$

The summation of rigid-body and deformation terms per polynomial order (Eq. (4)) is ideally equivalent to that of the desired trajectory (Eq. (5)). Since the actual compliant mechanism motion trajectory, $\Omega_c(\xi)$, and the model trajectory, $\Omega_e(\xi)$, may be considered equivalent (i.e., $\Omega_c(\xi) = \Omega_e(\xi)$), the error trajectory, $\Omega_c(\xi) - \Omega_d(\xi)$, may also be written as the difference $\Omega_e(\xi) - \Omega_d(\xi)$ (Eq. (6)).

$$\begin{aligned}
\delta(\Delta\xi) &= \Omega_e(\Delta\xi) - \Omega_d(\Delta\xi) \\
&= [k_{0,0} - d_0] + [(k_{1,0} + \boldsymbol{k_{0,1}}) - d_1]\Delta\xi \\
&\quad + [(k_{2,0} + \boldsymbol{k_{1,1}} + \boldsymbol{k_{0,2}}) - d_2]\Delta\xi^2 \\
&\quad + \ldots + \left[\left(k_{i,0} + \sum_{n=0}^{i-1}\boldsymbol{k_{n,i-n}}\right) - d_i\right]\Delta\xi^i \\
&\quad + \left[\left(\sum_{n=0}^{i}\boldsymbol{k_{n,i-n+1}}\right) - d_{i+1}\right]\Delta\xi^{i+1} \\
&\quad + \ldots + \left[\left(\sum_{n=0}^{i}\boldsymbol{k_{n,j-n}}\right) - d_j\right]\Delta\xi^j
\end{aligned} \tag{6}$$

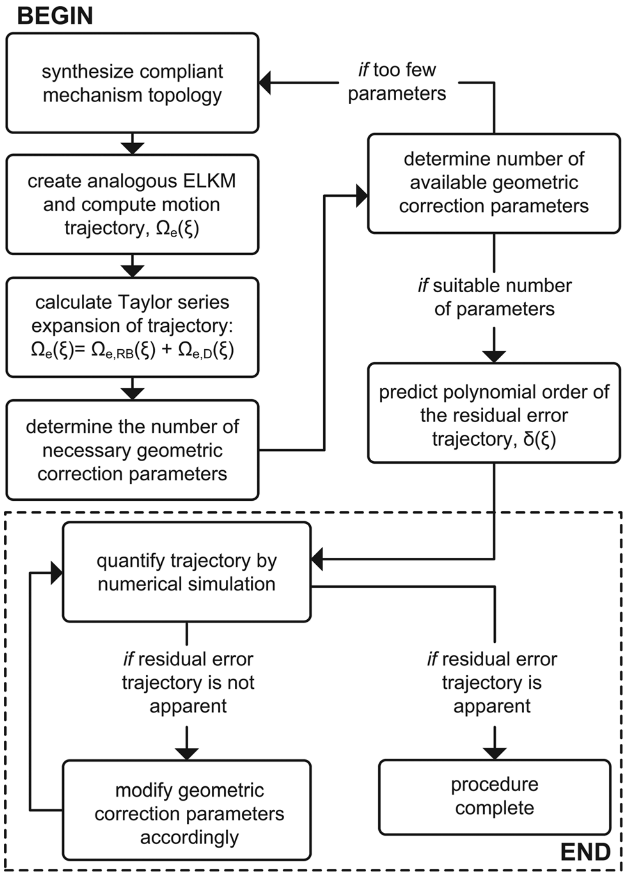

Fig. 4 Compliant mechanism design procedure utilizing the ELKM

Note that, as the magnitudes of the extensible components approach zero (i.e., $|\boldsymbol{f}(\xi)|\rightarrow 0$), the magnitudes of the deformation terms, $\boldsymbol{k}_{n,m>0}$, also approach zero (i.e., $\lim_{|f(\xi)|\rightarrow 0} \Omega_{e,D(\xi)}=0$). Here, the model's motion trajectory, $\Omega_{e(\xi)}$, approaches the rigid-body kinematic trajectory, $\Omega_{e,RB(\xi)}$. This limiting case corresponds to a limiting compliant mechanism shape: extreme lumped compliance, such that both the length and bending stiffness (i.e., thickness) of the compliant hinges approach zero. At this limit, the motion trajectory of the compliant mechanism, $\Omega_{c(\xi)}$, becomes equivalent to the motion trajectory of the rigid-body terms, $\Omega_{e,RB(\xi)}$.

An important observation here is that the deformation terms for any physical compliant mechanism will be nonzero; their *magnitudes* may only be minimized by lumped-compliance shapes or maximized by distributed-compliance shapes. And, these limits of compliance distribution are also typically bounded by practical considerations such as: (1) the material yield strain, given the range of mechanism actuation, $\xi-\xi_0$; (2) the available mechanism area (Fig. 1); and (3) the details of the chosen fabrication process. In contrast, the *magnitudes and signs* of the rigid-body terms are entirely determined by the locations of connection (i.e., kinematic constraint) between the segments comprising the compliant mechanism in its undeformed state, ξ_0; and these locations can be altered within the available mechanism area (Fig. 1) by design. Hence from a design perspective, the values of the rigid-body terms may be considered "completely specifiable by design," while the values of the deformation terms may be considered "partially specifiable by design."

By this insight, the procedure for minimizing the trajectory error (Eq. (6)) of a compliant mechanism—via modification of its topology—may be regarded as follows within the model framework: per polynomial order, the value of each rigid-body term is designed to compensate for the corresponding deformation terms so as to provide the correct overall motion trajectory of that order. In other words, the configuration of compliant segments (i.e., the mechanism topology) is designed to compensate for load-dependent trajectory components that arise during actuation. Within this context, Eq. (6) illustrates that the error trajectory only up to the ith order may be, in total or in part, redressed by modification of the mechanism topology. All trajectory components greater than or equal to the $(i+1)$th order are exclusively deformation terms, and are therefore, in principle, uncorrectable (i.e., only minimizable). By the nature of Taylor series expansions, it is likely that the $(i+1)$th order contribution will dominate that of any higher-order deformation terms over the finite actuation range, $\xi-\xi_0$.

Given a specific candidate compliant mechanism, the effectiveness of redressing the error trajectory can be determined by inspection of the rigid-body terms within the model. The formulation for each $k_{n,0}$ term indicates how its value may be modified by changing the initial lengths/orientations (i.e., l_0 in Eq. 1(*a*)). This thereby indicates how corresponding geometric changes to the compliant mechanism topology affect its trajectory, provided its shape remains largely invariant. Ideally, there would be i-number of unique geometric parameters available, each of which could be independently changed to modify the value of corresponding $k_{n,0}$ terms. In this case, the residual trajectory error would consist of significant $(i+1)$th to jth order polynomial components. Having less than i-number of suitable geometric modifications forces a tradeoff in the optimization procedure between the values of two or more $k_{n,0}$ terms in order to minimize the error trajectory.

Recall that increasing the distribution of compliance increases the magnitude of the deformation terms, $\boldsymbol{k}_{n,m>0}$, without affecting the value of the rigid-body terms, $k_{n,0}$. Regarding trajectory optimization, this indicates that a larger distribution in compliance may amount to more extensive geometric modifications and a larger magnitude residual error trajectory. Given material strain limitations, this implies a tradeoff between range of motion (i.e., increased by larger compliance distribution) and trajectory accuracy.

Overall, the extensible-link kinematic model illustrates a departure from classical rigid-link mechanism design, in which a desired motion trajectory is, in principle, traceable without error if fabrication is perfect. In contrast, Eq. (6) shows that the material deformation of a compliant mechanism during actuation can effectuate a load-dependent error trajectory, even if the topology and shape could be fabricated with perfect accuracy. Generally speaking, the model shows that, although material deformation in a compliant mechanism inherently provides motion repeatability, it is a source of trajectory error, which is critical in high-accuracy motion applications (Fig. 1).

The model is useful for understanding the qualitative motion characteristics of compliant mechanisms and for guiding the design process. Notably, developing this model framework required no assumptions or constraints regarding the compliant mechanism shape, material properties, or load application. These specifications are all contained within the extensible components, $\boldsymbol{f}(\xi)$, which, again, are generally nontrivial to express analytically. The practical utility of the model therefore comes from *not* having to specify explicit equations for the extensible components in order to identify load-independent and load-dependent motion components; and this makes it amenable to analysis of compliant mechanisms that cannot otherwise be represented in an analytical closed-form. For such cases, FE simulation can be used to infer the values of extensible components, $\boldsymbol{f}(\xi)$, and deformation terms, $\boldsymbol{k}_{n,m>0}$. This thereby enables minimization of the trajectory error by iterative modification of the geometric parameters identified within the model. This procedure is summarized below, and depicted in Fig. 4. Note that it may be analytical until the last step, where iterative numerical simulation is used to minimize the error trajectory (Fig. 4, dashed box).

(1) The formulations of the rigid-body terms, which constitute the trajectory $\Omega_{e,RB}(\xi)$, are determined by kinematic

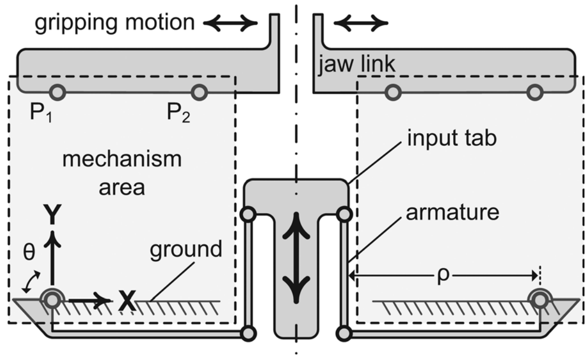

Fig. 5 Displacement-constraint design problem for parallel-jaw gripping mechanism, where mirror-image topologies fill right and left mechanism areas

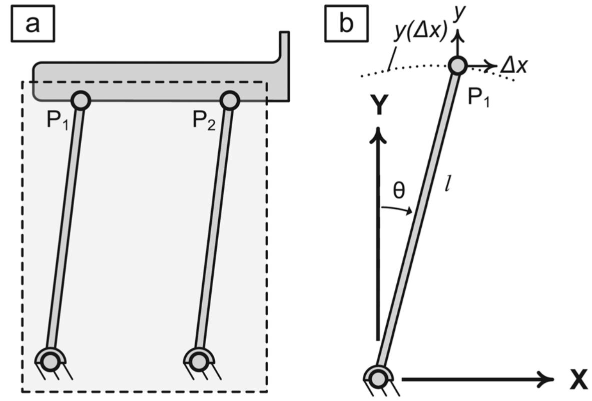

Fig. 6 The typical topology solution within the mechanism area (Fig. 5) is (*a*) a parallelogram, where (*b*) the trajectory of P_1 is constrained by a beam having extensible length *l*

analysis. The model (Fig. 3(*d*)) is derived based on the locations of connection between the segments that comprise the compliant mechanism at its undeformed state, ξ_0.

(2) The rigid-body terms are then analyzed to determine the geometric correction parameters. These parameters will correspond to the orientations and/or l_0 lengths of particular links at the undeformed state, ξ_0. If less than *i*-number of independent geometric parameters exist (Eq. (6)), a tradeoff must be determined between the values of two or more $k_{n,0}$ terms in the trajectory optimization procedure; and the designer may make a judgment call on whether to proceed with the current topology candidate, or to synthesize a new topology, resulting in a new extensible-link kinematic model. This step also enables the polynomial order of the residual error trajectory to be predicted (i.e., the error trajectory remaining after modification of the geometric parameters).

(3) The error trajectory is minimized via modification of the geometric parameters, where FE simulation is used to quantify the exact trajectory, $\Omega_e(\xi)$. Since the values of the rigid-body terms, $k_{n,0}$, are known analytically, fitting a *j*th-order polynomial curve to the FE simulated trajectory quantifies the net motion contribution of the deformation term(s) per polynomial order.

(4) The magnitude and sign of these net deformation term contributions inform the designer on how to modify each geometric correction parameter for the next FE simulation.

(5) This iteration may continue until: (1) the magnitude of the error trajectory is reduced below the design specifications; or (2) the polynomial order of the residual error trajectory becomes apparent, since this signifies the limit of trajectory correction—via modification of the geometric parameters—for the compliant mechanism.

3 Design of a Microgripper With Straight-Line Jaw Trajectory

3.1 Statement of Design Task. The utility and validity of the extensible-link kinematic model is now demonstrated by designing a compliant gripping mechanism with a straight-line parallel jaw trajectory. Straight-line jaw motion may be desired for micromechanical tension/compression tests [24], and for gripping soft objects such as cells [25], gels [26], and assemblies of micro and nanostructures [27]. These and other applications are sensitive to normal and shear forces, and therefore it is important to decouple these two loading conditions.

It is required that the compliant mechanism fits within the indicated mechanism area (Fig. 5, dashed box), and enables pure *X*-direction translation of the gripper jaw links without rotation. Translation of the jaw link in the *Y*-direction, as well as jaw link rotation, the constitute error trajectories. For practical use of this gripper in micromanipulation tasks, a 400 μm jaw actuation range (i.e., $\pm 100\,\mu$m *X*-displacement per jaw link) is desired, over which the *Y*-displacement of the jaw trajectory is less than 10 nm.

In order to achieve mirrored precision motion of both gripper faces, a single input motion provided by one actuator drives the actuation of both gripper jaws. This is enabled by the armature configuration (Fig. 5), which serves to translate linear motion of the input tab, provided by the actuator, to rotary motion, θ, about a grounded pivot. By design, the gripper jaw displacement may be proportional to the input tab displacement by means of a small angle approximation with respect to θ (Eq. (7)). This proportional relationship may be tuned based on armature length, ρ, which makes this configuration, and variants thereof, suitable for either amplifying the displacement of piezoelectric actuators or deamplifying the motion of classical linear actuators. The design task is therefore to determine a compliant mechanism topology that fits within the mechanism area, anchors at the available ground, and converts rotation of the grounded armature pivot, θ, to horizontal translation of the gripper jaws.

$$\theta = \theta_0 + \Delta\theta \quad \text{for :} \quad \Delta\theta : [-2\,\text{deg}, 2\,\text{deg}] \tag{7}$$

The location of the mechanism area (Fig. 5) is driven by two main considerations: (1) it is desirable to minimize the overall mechanism size; and (2) the mechanism area may not extend vertically above the jaw link, otherwise sample manipulation and viewing are obstructed. Note that this second consideration rules out the possibility of utilizing symmetry in the mechanism topology to achieve straight line motion. This design scenario is common in compliant gripping mechanism applications, and the typical solution is to utilize a parallelogram mechanism topology for guiding the jaw links (Fig. 6) [28–32]. In Sec. 3.2 , the precise motion characteristics and shortcomings of this topology are demonstrated within the context of the extensible-link model. Motivated by these findings, a new compliant mechanism topology is developed based on the classical Hoekens four-bar linkage that ensures improved trajectory accuracy. Presenting this design procedure illustrates the utility of the model for streamlining the selection and evaluation of candidate compliant mechanism topologies, as well as guiding the iterative procedure for optimizing the trajectory accuracy of the jaw in conjunction with FE simulation.

The suitability of both the parallelogram-based and Hoekens-based mechanisms for this application are evaluated with respect to the motion paths of points P_1 and P_2, which define the rigid-body trajectory of the jaw link. Here, the rigid-body translation of the jaw link is regarded as equivalent to the trajectory of P_1, and jaw link rotation as attributable to inaccurate duplication of the P_1 motion at P_2. Ideally, P_1 translates horizontally and this motion is perfectly duplicated at P_2. Separating rigid-body translation and rotation in this manner greatly simplifies the following analysis of the accuracy limits of gripper jaw trajectory.

It is important to keep in mind that the majority of the design process presented here is analytical. FE simulation is not unnecessary until the final design step, where it is utilized to iteratively modify geometric parameters identified within the compliant mechanism to minimize the error trajectory of the jaws (Fig. 10). These modifications were performed manually in the same CAD software program used to create the initial 2D compliant gripper contour. The CAD model was exported into ANSYS and meshed appropriately. Only 10s of nonlinear FE simulation iterations were necessary, meaning that the total time requirement for optimization amounted to less than half a day. The efficiency of this process is attributable to two main factors: (1) the appropriate geometry modifications as well as the polynomial order of the residual error trajectory were analytically determined before FE simulation; and (2) as a result, it was not necessary to implement an automated algorithmic optimization procedure, which may have taken more time and would not provide the same insights as to how the compliant mechanism topology affects the jaw error trajectory.

3.2 Parallelogram Mechanism

The trajectory of P_1 for the parallelogram topology is modeled by the pivoting of a beam with extensible length l (Fig. 6, Eq. (8)).

$$\mathbf{P_1} = \begin{bmatrix} x \\ y \end{bmatrix} = \begin{bmatrix} l\sin\theta \\ l\cos\theta \end{bmatrix} \tag{8}$$

It can be shown by kinematic analysis that the 2nd-order Taylor series expansion (i.e., $i=2$ in Eq. (3)) of the rigid-body P_1 trajectory, about the nominal position, θ_0, is sufficient to capture all significant motion contributions for small angular perturbations, $\Delta\theta$ (Eq. (7)). This may be written as a 2nd-order polynomial function, $y(\Delta x)$, in the global X-Y coordinate system (Eqs. (9) and (10)). Here, the y-direction motion is represented as a function of the gripping direction displacement, Δx (i.e., the stroke parameter), whereby the desired trajectory is: $y(\Delta x) = \text{constant}$ (i.e., horizontal translation of P_1).

$$y(\Delta x) = l\sqrt{1 - \left(\frac{l_0\sin\theta_0 + \Delta x}{l}\right)^2} \cong k_0 + k_1\Delta x + k_2\Delta x^2 \tag{9}$$

$$k_0 = \sqrt{l^2 - (l_0\sin\theta_0)^2} \tag{10a}$$

$$k_1 = \frac{-l_0\sin\theta_0}{\sqrt{l^2 - (l_0\sin\theta_0)^2}} \tag{10b}$$

$$k_2 = \frac{-l^2}{2\left(l^2 - (l_0\sin\theta_0)^2\right)^{3/2}} \tag{10c}$$

The decomposition $l = l_0 + f(\Delta x)$ (Eq. (1)) is now admitted for the k_n terms (Eq. (10)), where l_0 is the initial length and the extensible component, $f(\Delta x)$, is a smooth continuous function satisfying $f(0)=0$. Equation (11) is then constructed by Taylor series expansion of each k_n term about $\Delta x = 0$ for $j=3$ (referencing Eq. (3)), and collection of like-ordered terms. Here, it is clear that the 3rd-order trajectory component is, in principle, uncorrectable because it contains only deformation terms (notated in bold). It is therefore sufficient to truncate this series representation at $j=3$ because all higher-order terms are exclusively deformation terms, and will be dominated by this 3rd-order contribution over the stroke range (i.e., $\Delta x = \pm 100\,\mu$m). Note that it is not necessary to specify an explicit function for $f(\Delta x)$ to see the formulation of all $k_{n,m}$ terms (Eq. (12)). Moreover, the deformation terms, $\boldsymbol{k_{n,m>0}}$, are all of a form such that they require the existence of the extensible component to be non-zero-valued (Eqs. (12b)–(12d), (12f), (12g), and (12i)); and may contain only up to its mth-order derivative (i.e., $f^{(m)}(0)$). This is generally true regardless of the kinematic linkage arrangement (i.e., mechanism topology).

$$y(\Delta x) \cong k_{0,0} + \left[k_{1,0} + \boldsymbol{k_{0,1}}\right]\Delta x + \left[k_{2,0} + \boldsymbol{k_{1,1}} + \boldsymbol{k_{0,2}}\right]\Delta x^2 + \left[\boldsymbol{k_{2,1}} + \boldsymbol{k_{1,2}} + \boldsymbol{k_{0,3}}\right]\Delta x^3 \tag{11}$$

$$k_{0,0} = l_0\cos\theta_0 \tag{12a}$$

$$\boldsymbol{k_{0,1}} = \frac{f'(0)}{\cos\theta_0} \tag{12b}$$

$$\boldsymbol{k_{0,2}} = \frac{1}{2\cos\theta_0}f''(0) - \frac{\tan^2\theta_0}{2l_0\cos\theta_0}f'(0)^2 \tag{12c}$$

$$\boldsymbol{k_{0,3}} = \frac{1}{6\cos\theta_0}f'''(0) - \frac{\tan^2\theta_0}{2l_0\cos\theta_0}f''(0)f'(0) + \frac{\tan^2\theta_0}{2l_0\cos^3\theta_0}f'(0)^3 \tag{12d}$$

$$k_{1,0} = -\tan\theta_0 \tag{12e}$$

$$\boldsymbol{k_{1,1}} = \frac{\tan\theta_0}{l_0\cos^2\theta_0}f'(0) \tag{12f}$$

$$\boldsymbol{k_{1,2}} = \frac{\tan\theta_0}{2l_0\cos\theta_0}f''(0) - \frac{\tan\theta_0\left(2+\sin^2\theta_0\right)}{2l_0^2\cos^4\theta_0}f'(0)^2 \tag{12g}$$

$$k_{2,0} = \frac{-1}{2l_0\cos^3\theta_0} \tag{12h}$$

$$\boldsymbol{k_{2,1}} = \frac{1+2\sin^2\theta_0}{2l_0^2\cos^5\theta_0}f'(0) \tag{12i}$$

The rigid-body, $k_{n,0}$, terms (Eqs. (12a), (12e), and (12h)) are now inspected to determine the extent to which the trajectory error may be redressed by adjustment of the mechanism topology. The 1st-order error trajectory may be corrected since the magnitude and sign of $k_{1,0}$ may be designed to compensate for $k_{0,1}$ by modifying θ_0. However, for the 2nd-order trajectory, the only additional geometric parameter available in $k_{2,0}$ is l_0. The formulation of this term (Eq. (12 h)) shows that its magnitude, but not its sign, may be changed by modifying l_0; and this is true regardless of the shape of the corresponding segment in the compliant mechanism. Depending on how the mechanism deforms during actuator loading, it is possible that the 2nd-order trajectory error may not be redressable (i.e., if $\boldsymbol{k_{1,1}} + \boldsymbol{k_{0,2}} < 0$). Moreover, the inverse relationship between the magnitudes of $k_{2,0}$ and l_0 means that l_0 may become impractically large if small values of $k_{2,0}$ are required. This may therefore force a tradeoff between the values of $k_{1,0}$ and $k_{2,0}$ to minimize the error trajectory, even presuming perfect duplication of the P_1 trajectory at P_2. Ideally, two geometric parameters would be available that could be independently changed in a practical manner to control both the magnitude and sign of $k_{1,0}$ and $k_{2,0}$.

3.3 Hoekens-Derived Mechanism.

Now consider replacing beam l (Fig. 6) with a four-bar mechanism (Fig. 7). Here, the extensible-link kinematic model within the mechanism area consists of a closed four-bar mechanism (hashed shading) that defines the path of P_1, and a parallelogram-based mechanism that serves to replicate the motion of P_1 at P_2 (Fig. 7(a)). Again, the trajectory of P_1 is evaluated, which represents the translation of the jaw link. Referencing the classical Hoekens linkage as a starting point, the geometric parameters of the four-bar are defined as follows (Fig. 7(b)): a = crank, g = ground, b = follower, h = output, d = extension of h to P_1 at angle ψ. The vector trajectory of P_1 is written in the global X-Y coordinate system (Eq. (13)) such that it consists of the input crank angle, θ, defined with respect to the X-axis as shown, and the kinematic linkage arrangement (i.e., extensible link lengths and angle ψ). The expression for the internal angle, φ, is derived based on the kinematic constraint that the ends of link h must coincide with the respective ends of links a and b.

$$\mathbf{P_1} = \begin{bmatrix} x \\ y \end{bmatrix} = a\begin{bmatrix} \cos\theta \\ \sin\theta \end{bmatrix} + h\begin{bmatrix} \cos\varphi \\ \sin\varphi \end{bmatrix} + d\begin{bmatrix} \cos(\varphi+\psi) \\ \sin(\varphi+\psi) \end{bmatrix}$$
$$\varphi \triangleq \arcsin\left(\frac{b^2 - a^2 - h^2 - g^2 + 2ag\cos\theta}{\sqrt{(2ah\sin\theta)^2 + (2h(a\cos\theta - g))^2}}\right) - \arctan\left(\frac{a\cos\theta - g}{a\sin\theta}\right) \tag{13}$$

By kinematic analysis, the P_1 trajectory may expressed as the function, $y(\Delta x)$, in the global X-Y coordinate system, where its 2nd-order Taylor series expansion (i.e., $i=2$ in Eq. (3)) is sufficient to capture all significant motion contributions for small angular perturbations, $\Delta\theta$ (Eq. (7)). The series representation of $y(\Delta x)$ here is therefore identical in form to Eq. (11), but with the following equations for the rigid-body, $k_{n,0}$, terms (Eq. (14)). The equations for the deformation terms, $\boldsymbol{k_{n,m>0}}$, are not shown here because they are lengthy and their computation is not necessary within the context of the following trajectory optimization procedure.

$$k_{0,0} = \sqrt{1-R_0^2}(h_0 + d_0\cos\psi) + R_0 d_0 \sin\psi \tag{14a}$$

$$k_{1,0} = \frac{a_0 + g_0 - R_0(h_0 + d_0\cos\psi) + d_0\sqrt{1-R_0^2}\sin\psi}{\sqrt{1-R_0^2}(h_0 + d_0\cos\psi) + R_0 d_0\sin\psi} \tag{14b}$$

$$k_{2,0} = \frac{\left(\dfrac{R_0^2 h_0(a_0 - g_0) + R_0 g_0(a_0 + g_0) - h_0 a_0}{2h_0 a_0}\right)\dfrac{h_0 + d_0\cos\psi}{\sqrt{1-R_0^2}} - \left(\dfrac{R_0 h_0(a_0 - g_0) + g_0(a_0 + g_0)}{2h_0 a_0}\right) d_0\sin\psi}{\left(\sqrt{1-R_0^2}(h_0 + d_0\cos\psi) + R_0 d_0\sin\psi\right)^2}$$
$$R_0 \triangleq \frac{a_0^2 + h_0^2 + g_0^2 - b_0^2 + 2a_0 g_0}{2h_0(a_0 + g_0)} \tag{14c}$$

For brevity, these expressions (Eq. (14)) include the substitution $\theta_0 = 180\,\text{deg}$, which was determined, by inspection, to be requisite for a symmetric P_1 trajectory about the undeformed state of the mechanism. Here, symmetric trajectories occur for the following kinematic relationships: $\psi = 0^0$, $h_0 = b_0 = d_0$, considering equal angular perturbations of the crank (i.e., link a) about θ_0. Additionally, perfect horizontal straight-line motion (i.e., $k_{1,0} = k_{2,0} = 0$) is achieved for the following kinematic relationship: $h_0 = b_0 = d_0 = l_0$, such that $l_0/a_0 = 4$ and $g_0 = l_0 - a_0$. These link length relationships are slightly different than that of the classical Hoekens mechanism (i.e., $l_0/a_0 = 2.5$). To achieve the desired jaw range (0–400 μm) given the small-angle restriction (Eq. (7)), the link length $a_0 = 1.67$ mm is required, which is practically feasible.

Analysis of the rigid-body terms (Eq. (14)) reveals that both the sign and magnitude of $k_{1,0}$ and $k_{2,0}$ may be controlled by independently changing ψ and g_0, respectively (Fig. 8). Therefore, the 1st- and 2nd-order trajectory errors caused by the corresponding-order deformation terms may be completely corrected by proper modification of these two geometric parameters. Hence, the residual error trajectory of the gripper jaw is predicted to be a 3rd-order polynomial that is, in principle, not correctable. Note that, even though the 3rd-order rigid-body term (i.e., $k_{3,0}$) is negligible, the cumulative contribution from the 3rd-order deformation terms (i.e., $\boldsymbol{k_{2,1}} + \boldsymbol{k_{1,2}} + \boldsymbol{k_{0,3}}$) may be significant in magnitude.

So far, only the trajectory of P_1 has been considered. To achieve the desired gripper jaw motion, the P_1 trajectory must be duplicated at P_2 by the parallelogram linkage portion of the mechanism (Fig. 7(*a*)). The above analysis may be performed for this parallelogram linkage as well in order to express the motion of P_2 in a parametric form. But, for brevity and clarity, it is simply noted that all significant contributions to the trajectory of P_2 may be captured in the form on Eq. (11) because all links in the parallelogram linkage are subject to the small angle constraint (Eq. (7)). Therefore, by analogy, adjusting ϕ (Fig. 7(*a*)) modifies the linear trajectory of P_2. This angle will be optimized in order to minimize gripper jaw rotation, ω; and as the FE results will show, this linear correction of the P_2 trajectory is sufficient.

The Hoekens-based kinematic mechanism (Fig. 7(*a*)) is translated into a lumped-compliance flexure mechanism (Fig. 9) now that all suitable geometric modifications have been determined. Here, the geometric centers of thin compliant hinges (Fig. 9) coincide with the locations of the pin joints in the kinematic model (Fig. 7(*a*)). The hinges have a cycloidal profile [33] which, compared to other compliant hinge contours, maximizes in-plane rotational compliance and translational stiffness for a prescribed angular deflection limit (Eq. (7)) and allowable material strain. For microfabrication of the gripper from a silicon wafer, a strain limit of 0.5% [34] is chosen. Note that a lumped-compliance shape has been chosen in order to minimize the magnitude of the deformation terms, $\boldsymbol{k_{n,m>0}}$, and thereby the magnitude of the residual error trajectory.

The jaw trajectory of the compliant mechanism is now optimized by iterative manual adjustment of the geometric parameters (i.e., $\Delta\psi$, Δg_0, $\Delta\phi$) and evaluated using nonlinear FE simulation in ANSYS. The rotation (Fig. 10(*a*)) and translation (Fig. 10(*b*)) of the jaw over the stroke, Δx, are plotted for the initial (*) and final (o) FE simulations. The compliant mechanism for the initial simulation has model link lengths corresponding to $k_{1,0} = k_{2,0} = 0$, and therefore the error trajectory here is entirely attributable to the deformation terms, $\boldsymbol{k_{n,m>0}}$, in the model. The polynomial curves fitted to the jaw rotation, $\omega(\Delta x)$, and P_1 trajectory, $y(\Delta x)$, quantify the net deformation-term motion contribution per polynomial order, which informs the designer on how to modify the geometric parameters (i.e., $\Delta\psi$, Δg_0, $\Delta\phi$) to minimize the error trajectory. The results from the initial FE simulation (Figs. 10(*a*) and 10(*b*), asterisks) indicate the following modifications: increase ϕ with respect to ψ to redress jaw rotation [16]; decrease ψ and g_0 to redress jaw translation errors (Fig. 8). All three geometric parameters may be modified at once.

The influence of these modifications is evaluated by subsequent FE simulation, and iteration continues until the polynomial order of the predicted residual error trajectory becomes apparent. To illustrate the validity of this model, an intermediate step is also shown where only the linear trajectory component of P_1 (i.e., $\Delta\psi$) is corrected, resulting in a parabolic error trajectory (Fig. 10(*b*), triangles). It is to be noted that the deformation terms, $\boldsymbol{k_{n,m>0}}$, include initial link lengths (i.e., l_0 in Eq. (1*a*)) as well as extensible components, $\boldsymbol{f(\xi)}$, and therefore their magnitude is partially dependent on the undeformed state of the mechanism. This

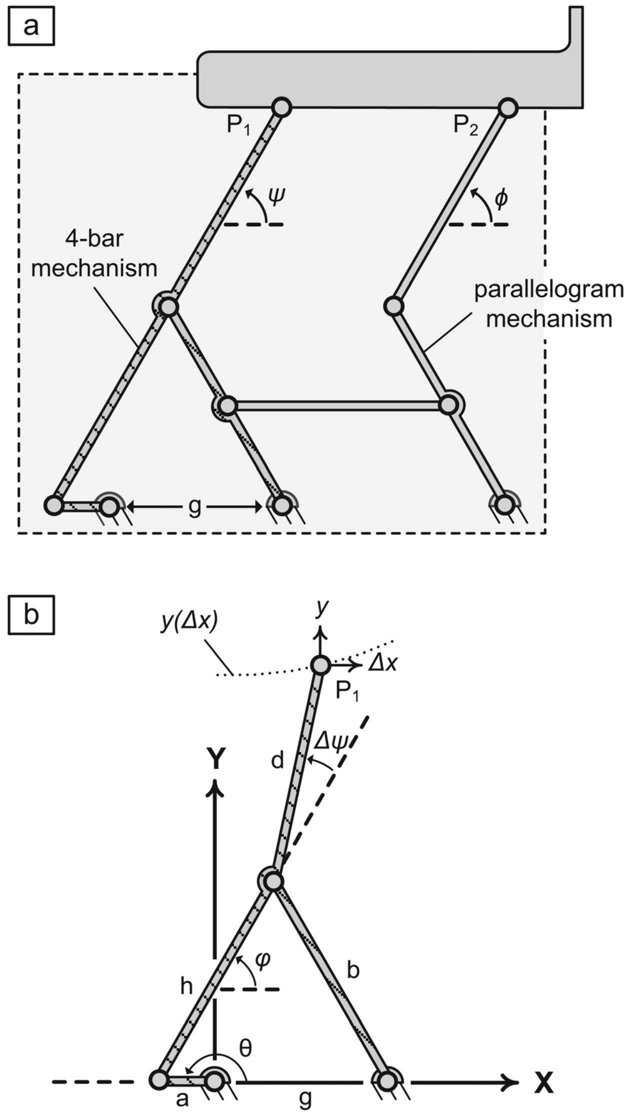

Fig. 7 (*a*) Mechanism solution for straight-line horizontal jaw displacement, which utilizes (*b*) a four-bar mechanism based on the Hoeken's linkage to determine the motion of P_1

implies that the trajectory error correction procedure here is inherently iterative because modifying the geometric parameters changes the value of the rigid-body terms and deformation terms.

Fewer than 30 iterations were required to optimize the jaw trajectory, and the final geometric modifications with respect to the initial topology, as denoted in Fig. 9, were: $\Delta\psi = -0.850\,\text{deg}$, $\Delta g_0 = -0.7\,\text{mm}$, $\Delta\phi = -0.354\,\text{deg}$. The final compliant gripper exhibits jaw rotation less than $0.8\,\mu\text{rad}$ and translation error less than 5 nm over the entire stroke according to the final FE simulation (Figs. 10(*a*)–10(*c*); circles). The residual error trajectory of the gripper jaw is 3rd-order, as predicted (Fig. 10(*c*)). This is therefore the limit of trajectory error correction for the compliant microgripper (Fig. 9).

4 Summary and Discussion

Within the proposed model framework, the error trajectory of a compliant mechanism may generally include both load-independent and load-dependent components (Eq. (6)). The rigid-body terms, $k_{n,0}$, comprise a load-independent trajectory component, $\Omega_{\text{e,RB}}(\xi)$, that is attributable to only the mechanism's topology, irrespective of the mechanism shape. The deformation terms, $\boldsymbol{k_{n,m>0}}$, comprise a load-dependent component, $\Omega_{\text{e,D}}(\xi)$,

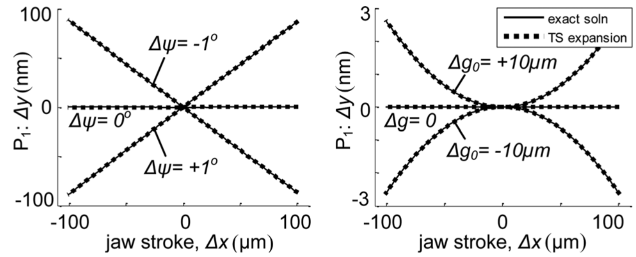

Fig. 8 Modifications of geometric parameters $\Delta\Psi$ and Δg_0 correct 1st- and 2nd-order P_1 trajectory errors, respectively. The trajectory is plotted as: $\Delta y = y(\Delta x) - k_{0,0}$.

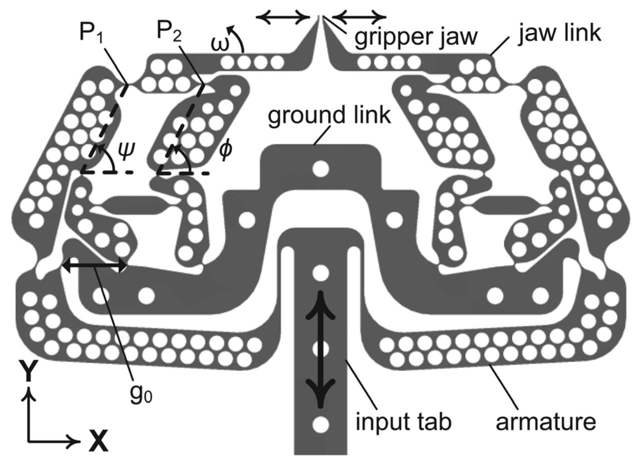

Fig. 9 Lumped-compliance gripper with straight-line parallel-jaw trajectory based on the Hoekens four-bar linkage

that is determined by the mechanism's topology and shape, as well as the applied load and material properties.

Modification of the mechanism topology alone (i.e., shape remains invariant) may redress trajectory errors up to the ith order, provided that i-number of geometric parameters exist within the model framework (i.e., by analysis of the $k_{n,0}$ terms in Eq. (6)). Having less than i-number of suitable geometric parameters forces a tradeoff between the values of two or more $k_{n,0}$ terms in the optimization procedure, regardless of the mechanism shape—and alleviation of this tradeoff would require a different mechanism topology.

Modification of the compliant mechanism's shape, on the other hand, only affects the magnitude of the load-dependent trajectory component. Within the model, the shape of the segments comprising the compliant mechanism (Figs. 2(*b*) and 2(*c*)) affects the extensible components, $\boldsymbol{f(\xi)}$, but not the initial lengths, l_0, that define the mechanism topology. Moreover, error trajectories of at least $(i+1)^{\text{th}}$ order are composed exclusively of deformation terms, $\boldsymbol{k_{n,m>0}}$, and therefore require compensatory loading to be completely redressed—recall that lumped-compliance shapes may minimize, but not eliminate, load-dependent trajectory components. This is illustrated in the case study, wherein the residual error trajectory of the gripper jaw exhibits a dominant polynomial order of: $(i+1) = 3$ (Fig. 10(*c*)). It is therefore entirely load-dependent and uncorrectable by topology modification alone (i.e., modification of the geometric parameters: $\Delta\psi$, Δg_0, $\Delta\phi$), and will exist irrespective of the compliant mechanism shape.

It is important to realize that the presented model does not assume or impose the motion of a rigid-body kinematic linkage (i.e., as in PRBM). Model construction consists of: (1) identifying particular material points in the compliant mechanism that represent locations of connection between segments comprising

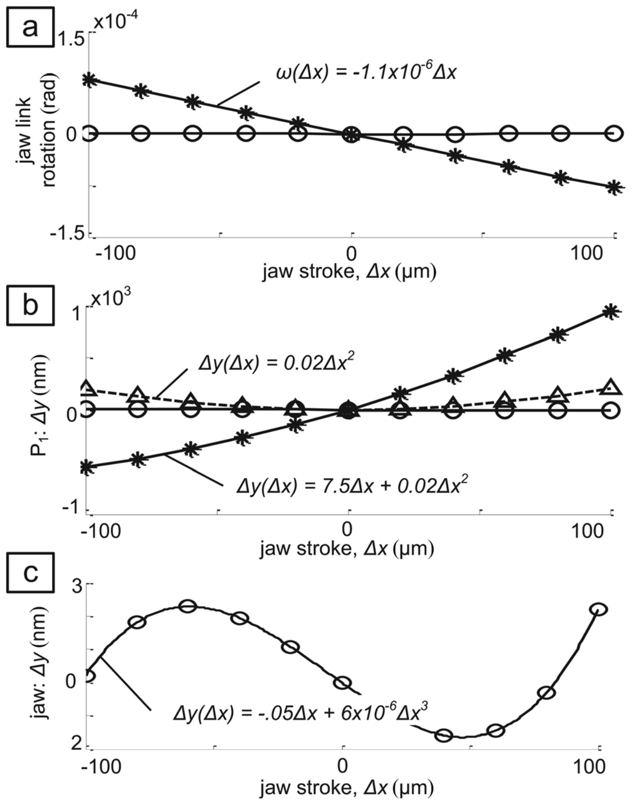

Fig. 10 Demonstration of reduced jaw trajectory error in (*a*) jaw link rotation over the jaw stroke, Δx, between initial (*) and optimized (o) FE simulations; and (*b*) P_1 trajectory over jaw stroke between initial (*), 1st-order optimized only (Δ), and fully optimized (o) FE simulations. (*c*) The optimized jaw trajectory exhibits a residual 3rd-order error, as predicted. The trajectories in (*b,c*) are plotted as: $\Delta y = y(\Delta x) - k_{0,0}$.

the topology; and (2) composing the trajectory, $\Omega_e(\xi)$ (Eq. (2)), in terms of the vectorial distances, l, between these material points. The ability to separate load-independent, $\Omega_{e,RB}(\xi)$, and load-dependent, $\Omega_{e,D}(\xi)$, components in the Taylor series expansion of the trajectory, $\Omega_e(\xi)$ (Eq. (3)), is simply a consequence of admitting the decomposition of Eq. (1). Remarkably, the load-independent trajectory component, $\Omega_{e,RB}(\xi)$, is equivalent to the trajectory of the rigid-body kinematic linkage corresponding to the undeformed state, ξ_0, of the compliant mechanism topology (i.e., as if all $\boldsymbol{f(\xi)} \equiv 0$).

While the extensible components, $\boldsymbol{f(\xi)}$, (and therefore the deformation terms) are generally nontrivial to calculate, the calculation for the load-independent trajectory, $\Omega_{e,RB}(\xi)$, is exact and independent of the compliant mechanism shape, as it depends only on the l_0 lengths. Herein lies the practical utility of the model because the contributions of topology versus shape to the compliant mechanism's trajectory may be distinguished by: (1) noting the existence of significant deformation terms and (2) calculating only $\Omega_{e,RB}(\xi)$. This is illustrated in the case study, wherein analysis and minimization of the gripper jaw's error trajectory (Fig. 10) required only Eqs. (11) and (14) despite the complicated shape of the microgripper (Fig. 9). The proposed model may also, without difficulty, be extended to three dimensions, as well as to compliant mechanisms with multiple input loads and/or output trajectories.

Last, it is recognized that some ambiguity exists in the selection of material points representing locations of connection which may enable variation, between designers, in the partitioning of a compliant mechanism into segments (Figs. 2(*b*) and 2(*c*)); and this variation results from a designer's interpretation of a compliant mechanism's topology versus shape. The important point is that the proposed model shows how the configuration of segments—as identified by the designer—affects the motion trajectory of the compliant mechanism. While it is, in principle, possible to compute the vector algebra between an arbitrary set of selected material points, design insight is only gained if the locations of the selected material points unambiguously represent the positions of corresponding geometric features in the compliant mechanism. For example, it would be inappropriate to select a material point in the middle of segment b or d (Figs. 3(*a*) and 3(*b*)) because arbitrary adjustment of its position would not correspond to a clear modification of the compliant mechanism topology—as is typically the case with the locations of hinge centers (Fig. 2(*b*)) and beam ends (Fig. 2(*c*)).

5 Conclusion

We have developed an analytical model for understanding the motion characteristics of an arbitrary planar compliant mechanism. The model is composed of extensible vectorial lengths, l, which represent the configuration of compliant segments comprising the mechanism; whereby the motion trajectory is constructed as an analytical function in terms of these vectorial lengths. Utilizing Taylor series expansion, the trajectory is separated into motion components that are either: (1) load-independent and entirely specifiable by the mechanism topology (i.e., *rigid-body* terms); or (2) load-dependent and represent all load-geometry interdependencies that arise during mechanism actuation (i.e., *deformation* terms). A compliant microgripper (Fig. 9) is designed in the case study, which demonstrates the utility of this model for streamlining the compliant mechanism design and trajectory optimization processes, in conjunction FE simulation. As demonstrated in the case study, the model is particularly useful for nonsymmetric mechanism topologies with shapes that are too complex to represent in an analytical closed form.

Acknowledgment

J.B. was supported by a National Science Foundation Graduate Research Fellowship. Additional support to J.B. and A.J.H. was provided by the Office of Naval Research (N000141010556).

Nomenclature

ξ = stroke parameter
ξ_0 = stroke parameter at the undeformed state of the mechanism
$\xi - \xi_0$ = actuation range
l = extensible link length
l_0 = initial length of l (corresponding to ξ_0)
$\boldsymbol{f(\xi)}$ = extensible component of l
$\Omega_d(\xi)$ = desired motion trajectory
$\Omega_c(\xi)$ = compliant mechanism motion trajectory
$\delta(\xi)$ = error trajectory
$\Omega_e(\xi)$ = model motion trajectory
$\Omega_{e,RB}(\xi)$ = load-independent component of model motion trajectory
$\Omega_{e,D}(\xi)$ = load-dependent component of model motion trajectory
$k_{n,0}$ = rigid-body terms (that comprise $\Omega_{e,RB}(\xi)$)
$\boldsymbol{k_{n,m>0}}$ = deformation terms (that comprise $\Omega_{e,D}(\xi)$)

References

[1] Culpepper, M. L., and Anderson, G., 2004, "Design of a Low-Cost Nano-Manipulator Which Utilizes a Monolithic, Spatial Compliant Mechanism," Precis. Eng., **28**(4), pp. 469–482.
[2] Tian, Y., Shirinzadeh, B., and Zhang, D., 2010, "Design and Dynamics of a 3-DOF Flexure-Based Parallel Mechanism for Micro/Nanomanipulation," Microelectron. Eng., **87**(2), pp. 230–241.
[3] Chen, S. C., and Culpepper, M. L., 2006, "Design of a Six-Axis Micro-Scale Nanopositioner—mu HexFlex," Precis. Eng., **30**(3), pp. 314–324.
[4] Lantz, M. A., Rothuizen, H. E., Drechsler, U., Haberle, W., and Despont, M., 2007, "A Vibration Resistant Nanopositioner for Mobile Parallel-Probe Storage Applications," J. Microelectromech. Syst., **16**(1), pp. 130–139.

[5] Ho, C. M., and Tai, Y. C., 1998, "Micro-Electro-Mechanical-Systems (MEMS) and Fluid Flows," Annu. Rev. Fluid Mech., **30**, pp. 579–612.
[6] Beeby, S. P., Tudor, M. J., and White, N. M., 2006, "Energy Harvesting Vibration Sources for Microsystems Applications," Meas. Sci. Technol., **17**(12), pp. R175–R195.
[7] Hu, Y. H., Lin, K. H., Chang, S. C., and Chang, M., 2008, "Design of a Compliant Micromechanism for Optical-Fiber Alignment," *Measurement Technology and Intelligent Instruments VIII*, W. Gao, Y. Takaya, Y. Gao, M. Krystek, eds., Trans Tech Publications Ltd, Stafa-Zurich, pp. 141–144.
[8] Chen, S. C., Culpepper, M. L., and Jordan, S., "Six-Axis Compliant Mechanisms For Manipulation of Micro-Scale Fiber Optics Components—Art. No. 64660P," Proc. Conference on MOEMS and Miniaturized Systems VI, SPIE-Int Soc Optical Engineering, pp. P4660–P4660.
[9] Lee, C. W., and Kim, S. W., 1997, "An Ultraprecision Stage For Alignment of Wafers in Advanced Microlithography," Precis. Eng., **21**(2–3), pp. 113–122.
[10] Meli, F., and Thalmann, R., 1998, "Long-Range AFM Profiler Used for Accurate Pitch Measurements," Meas. Sci. Technol., **9**(7), pp. 1087–1092.
[11] Kim, D., Lee, D. Y., and Gweon, D. G., 2007, "A New Nano-Accuracy AFM System for Minimizing Abbe Errors and the Evaluation of its Measuring Uncertainty," Ultramicroscopy, **107**(4–5), pp. 322–328.
[12] Qin, D., Xia, Y. N., Rogers, J. A., Jackman, R. J., Zhao, X. M., and Whitesides, G. M., 1998, "Microfabrication, Microstructures and Microsystems," Microsyst. Technol. Chem. Life Sci., **194**, pp. 1–20.
[13] Howell, L. L., and Midha, A., 1995, "Parametric Deflection Approximations for End-Loaded Large-Deflection Beams in Compliant Mechanisms," ASME J. Mech. Des., **117**(1), pp. 156–165.
[14] Howell, L. L., and Midha, A., 1994, "A Method for The Design of Compliant Mechanisms With Small-Length Flexural Pivots," ASME J. Mech. Des., **116**(1), pp. 280–290.
[15] Awtar, S., and Slocum, A. H., 2007, "Constraint-Based Design of Parallel Kinematic XY Flexure Mechanisms," ASME J. Mech. Des., **129**(8), pp. 816–830.
[16] Awtar, S., Slocum, A. H., and Sevincer, E., 2007, "Characteristics of Beam-Based Flexure Modules," ASME J. Mech. Des., **129**(6), pp. 625–639.
[17] Awtar, S., and Sen, S., 2010, "A Generalized Constraint Model for Two-Dimensional Beam Flexures: Nonlinear Load-Displacement Formulation," ASME J. Mech. Des., **132**(8), p. 081008.
[18] Frecker, M. I., Ananthasuresh, G. K., Nishiwaki, S., Kikuchi, N., and Kota, S., 1997, "Topological Synthesis of Compliant Mechanisms Using Multi-Criteria Optimization," ASME J. Mech. Des., **119**(2), pp. 238–245.
[19] Saxena, A., and Ananthasuresh, G. K., 2000, "On an Optimal Property of Compliant Topologies," Struct. Multidiscip. Optim., **19**(1), pp. 36–49.
[20] Carbonari, R. C., Silva, E. C. N., and Nishiwaki, S., 2005, "Design of Piezoelectric Multi-Actuated Microtools Using Topology Optimization," Smart Mater. Struct., **14**(6), pp. 1431–1447.
[21] Matsui, K., and Terada, K., 2004, "Continuous Approximation of Material Distribution for Topology Optimization," Int. J. Numer. Methods Eng., **59**(14), pp. 1925–1944.
[22] Tai, K., and Chee, T. H., 2000, "Design of Structures and Compliant Mechanisms by Evolutionary Optimization of Morphological Representations of Topology," J. Mech. Des., **122**(4), pp. 560–566.
[23] Lu, K. J., and Kota, S., 2006, "Topology and Dimensional Synthesis of Compliant Mechanisms Using Discrete Optimization," ASME J. Mech. Des., **128**(5), pp. 1080–1091.
[24] Dimiduk, D. M., Uchic, M. D., and Parthasarathy, T. A., 2005, "Size-Affected Single-Slip Behavior of Pure Nickel Microcrystals," Acta Mater., **53**(15), pp. 4065–4077.
[25] Loh, O., Vaziri, A., and Espinosa, H., 2009, "The Potential of MEMS for Advancing Experiments and Modeling in Cell Mechanics," Exp. Mech., **49**(1), pp. 105–124.
[26] Ahn, S. K., Kasi, R. M., Kim, S. C., Sharma, N., and Zhou, Y. X., 2008, "Stimuli-Responsive Polymer Gels," Soft Matter, **4**(6), pp. 1151–1157.
[27] Cao, A. Y., Dickrell, P. L., Sawyer, W. G., Ghasemi-Nejhad, M. N., and Ajayan, P. M., 2005, "Super-Compressible Foamlike Carbon Nanotube Films," Science, **310**(5752), pp. 1307–1310.
[28] Tsai, Y. C., Lei, S. H., and Sudin, H., 2005, "Design and Analysis of Planar Compliant Microgripper Based on Kinematic Approach," J. Micromech. Microeng., **15**(1), pp. 143–156.
[29] Nah, S. K., and Zhong, Z. W., 2007, "A Microgripper Using Piezoelectric Actuation for Micro-Object Manipulation," Sens. Actuators A, **133**(1), pp. 218–224.
[30] Zubir, M. N. M., Shirinzadeh, B., and Tian, Y. L., 2009, "A New Design of Piezoelectric Driven Compliant-Based Microgripper for Micromanipulation," Mech. Mach. Theory, **44**(12), pp. 2248–2264.
[31] Zubir, M. N. M., and Shirinzadeh, B., 2009, "Development of a High Precision Flexure-Based Microgripper," Precis. Eng., **33**(4), pp. 362–370.
[32] Goldfarb, M., and Celanovic, N., 1999, "A Flexure-Based Gripper for Small-Scale Manipulation," Robotica, **17**, pp. 181–187.
[33] Tian, Y., Shirinzadeh, B., Zhang, D., and Zhong, Y., 2010, "Three Flexure Hinges For Compliant Mechanism Designs Based on Dimensionless Graph Analysis," Precis. Eng., **34**(1), pp. 92–100.
[34] Ando, T., Sato, K., Shikida, M., Yoshioka, T., Yoshikawa, Y., Kawabata, T., and Ieee, I., 1997, "Orientation-Dependent Fracture Strain in Single-Crystal Silicon Beams Under Uniaxial Tensile Conditions," Mhs'97: Proceedings of 1997 International Symposium on Micromechatronics and Human Science.